Three-dimensional reconstruction of stained histological slices and 3D non-linear registration with *in-vivo* MRI for whole baboon brain

Julien Dauguet [a,b,*], Thierry Delzescaux [a], Françoise Condé [c], Jean-François Mangin [a], Nicholas Ayache [b], Philippe Hantraye [a,c], Vincent Frouin [a]

[a] *Service Hospitalier Frédéric Joliot, CEA, Orsay, France*
[b] *INRIA, Epidaure/Asclepios Project, Sophia Antipolis, France*
[c] *CNRS, URA 2210, Orsay, France*

Abstract

The correlation between *post-mortem* data and *in-vivo* brain images is of high interest for studying neurodegenerative diseases. This paper describes a protocol that matches a series of stained histological slices of a baboon brain with an anatomical MRI scan of the same subject using an intermediate 3D-consistent volume of "blockface" photographs taken during the sectioning process.

Each stained histological section of the baboon brain was first registered to its corresponding blockface photograph using a novel "hemi-rigid" transformation. This piecewise rigid 2D transformation was specifically adapted to the registration of slices which contained both hemispheres. Subsenquently, to correct the global 3D deformations of the brain caused by histological preparation and fixation, a 3D elastic transformation was estimated between the blockface volume and the MRI data. This 3D elastic transformation was then applied to the histological volume previously aligned using the hemi-rigid method to complete the registration of the series of stained histological slices with the MRI data.

We assessed the efficacy of our method by evaluating the quality of matching of anatomical features as well as the difference of volume measurements between the MRI and the histological images. Two complete baboon brains (with the exception of cerebellum) were successfully processed using our protocol.
© 2007 Elsevier B.V. All rights reserved.

Keywords: 3D reconstruction; Histology; primate; *In-vivo/post-mortem* registration; PMI; Hemi-rigid

Recently, biomedical imaging has been increasingly utilized in research to study brain and its associated dysfunctions. Medical imaging provides valuable *in-vivo* information particularly in diagnosing diseases and in guiding therapies. However, histological analysis is still the gold-standard for the accurate description of neuroanatomy and for tissue characterization of the brain. Therefore, mapping histological data on *in-vivo* data, the ultimate geometric reference for analysis, is of high interest for the biomedical community. This is a challenge because of the many differences between the brain in its original geometry and the resulting series of 2D histological slices.

Non-human primates were used in this study because their brain structure and functions are comparable to a human's. In addition, the brain size of most non-human primates is large enough to be imaged with an acceptable resolution in the same *in-vivo* scanners used for humans.

Generally speaking, there are two types of brain deformations caused by histological preparation and fixation: global 3D deformation and slice-specific 2D deformations. Global 3D deformations caused by the extraction of the brain from the skull include (1) global shrinkage due to the loss of cerebro spinal fluid, loss of blood irrigation, and global dehydration, and (2) various deformations due to gravity or other mechanical effects, and possible specific processings (such as fixation and paraffin embedding). We defined these global three-dimensional deformations as "primary deformations" because they are first to appear and they occur before sectioning the brain. In order to correct these deformations, it is necessary to estimate a 3D

* Corresponding author at: Computational Radiology Laboratory, Harvard Medical School, Children's Hospital, 300 Longwood Ave, Boston, MA 02115, USA. Tel.: +1 617 355 5432; fax: +1 617 582 6033.

E-mail addresses: dauguet@crl.med.harvard.edu (J. Dauguet), thierry.delzescaux@cea.fr (T. Delzescaux).

transformation between the brain in its *post-mortem* geometry and the actual *in-vivo* brain.

The individual 2D deformations for each slice are due to the serial sectioning of the brain into 2D slices, and include: (1) specific deformations due to cutting (shearing, tearing), (2) shrinkage due to temperature changes (see Gardella et al., 2003, for a quantitative study of deformations), and (3) changes in the original geometry of each slice due to the mounting on glass slides of both hemispheres and displacements of smaller parts like gyri. We defined these individual 2D deformations as "secondary deformations" because they appear during the cutting step, after the primary deformations. The correction of these deformations requires first the estimation of the initial spatial 2D configuration of each slice, second the reconstruction of the 3D volume by alignment of the series of slices.

The correction of these two different types of deformations that will ultimately link the analysis of histology and MRI can benefit from the use of an intermediate modality. This intermediate modality consists of photographs or videos of the brain face taken during the sectioning process (Toga et al., 1994; Kim et al., 1997; Mega et al., 1997; Ourselin et al., 2001; Bardinet et al., 2002), which are usually called blockface photographs. This intermediate modality is used in this study.

Correction of the secondary deformations previously described leads to the 3D reconstruction. Many works have been done on the alignment of series of 2D slices, using global affine transformations (Hibbard and Hawkins, 1988; Andreasen et al., 1992; Zhao et al., 1993; Goldszal et al., 1995; Schormann et al., 1995; Rangarajan et al., 1997; Cohen et al., 1998; Ourselin et al., 2001; Bardinet et al., 2002; Malandain et al., 2004; Dauguet et al., 2005) or non-linear transformations (Kim et al., 1997; Mega et al., 1997; Schormann and Zilles, 1998; Pitiot et al., 2006; Chakravarty et al., 2006). However, none of these works proposed a specifically dedicated solution for the separation of hemispheres. Furthermore, existing works concerning 3D reconstruction and *in-vivo* matching often considered only one single hemisphere, or a sub-region of a hemisphere, since one half of the brain is frequently used for other procedures (such as binding) which are not compatible with serial sectioning. Common solutions to cope with separated hemispheres are to assume the hemispheres did not have independent motions, to manually separate and extract each hemisphere into different images, or to use global non-linear transformations.

Registration of complete brain slices with independent rigid transformations for each hemisphere is not a trivial problem. The most intuitive way to proceed would be to segment each hemisphere on each image and then perform individual registration for each pair of corresponding hemispheres. However, the segmentation is challenging since, on each slice, the hemispheres can be either connected or split into several parts. The pairing of the corresponding hemispheres is therefore non-trivial and it is not guaranteed that the segmentations of the hemispheres on the two images will be consistent, especially if they are multimodal images. Moreover, the registration of each hemisphere separately is not robust because only half of the information is being used. The "hemi-rigid" method we propose here can offer an adaptive solution to these problems: an automatic seg-

mentation of the hemispheres is performed on only one of the two images to register, and the robustness of the registration is improved by a coarse to fine approach. The blockface volume is used as reference for the positioning of the hemispheres within each histological slice.

The correction of the primary deformations leads to the 3D *post-mortem/in-vivo* matching. To estimate 3D transformations for the registration of two brains, several techniques have been proposed in the literature, either performing rigid transformations using mutual information as similarity criterion (Viola and Wells, 1997; Maes et al., 1997), or non-linear transformations (Ashburner and Friston, 1997; Friston et al., 1995; Davatzikos, 1997; Collins and Evans, 1998; Thirion, 1998; Christensen, 1999; Cachier et al., 2003; Clatz et al., 2005). A more complete overview of medical image registration can be found in Maintz and Viergever (1998). For the particular 3D registration of *post-mortem* and *in-vivo* primate brains, different strategies have been proposed in the literature. Ourselin et al. (2001) and Bardinet et al. (2002) have proposed an affine 3D transformation for the registration of the basal ganglia. For global matching of one hemisphere, Malandain et al. (2004) proposed a method based on an alternated correction of primary and secondary deformations using 3D and 2D affine registrations. Schormann et al. (1995) used an optimized affine registration of labeled regions to correct the deformations between histological slices and the MRI section. Thompson and Toga (1996) developed a 3D warping method based on surface that was used in 2D for histology registration in Mega et al. (1997). A 3D viscous fluid transformation model has been proposed by Christensen et al. (1997) and applied to the deformation of blockface photographs, whereas Schormann and Zilles (1998) performed a 3D transformation based on the elastic medium theory with a full-multigrid strategy. Elastic methods using thin plate splines with control points have been proposed to be used for rodent brains (Kim et al., 1997), which do not, however, present the same deformations as that of primate brains.

The protocol proposed here aims to separately correct the primary and the secondary deformations (listed in Fig. 1) for the whole primate brain. An intuitive way to achieve this is to apply corrections in the reverse order than the original deformations occurred.

1. Material and methods

Two adult baboons (*Papio papio*) involved in a study concerning the implantation of a cortical electrode for Parkinson's disease (see Drouot et al., 2004, for more details) were processed. An *in-vivo* T1 MRI scan was acquired for each baboon using a 1.5 T magnet (General Electric Medical Systems, Waukesha, WI) with a resolution of 0.78 mm × 0.78 mm × 1 mm.

The brain of each baboon was fixed by transcardial perfusion of 4% paraformaldehyde (PFA). The brains were divided into three blocks in the coronal orientation because first, the brain volumes were too big for the Leica microtome we used for sectioning and second because post-fixation with PFA is better on small parts rather than on the full brain (especially for deep inner
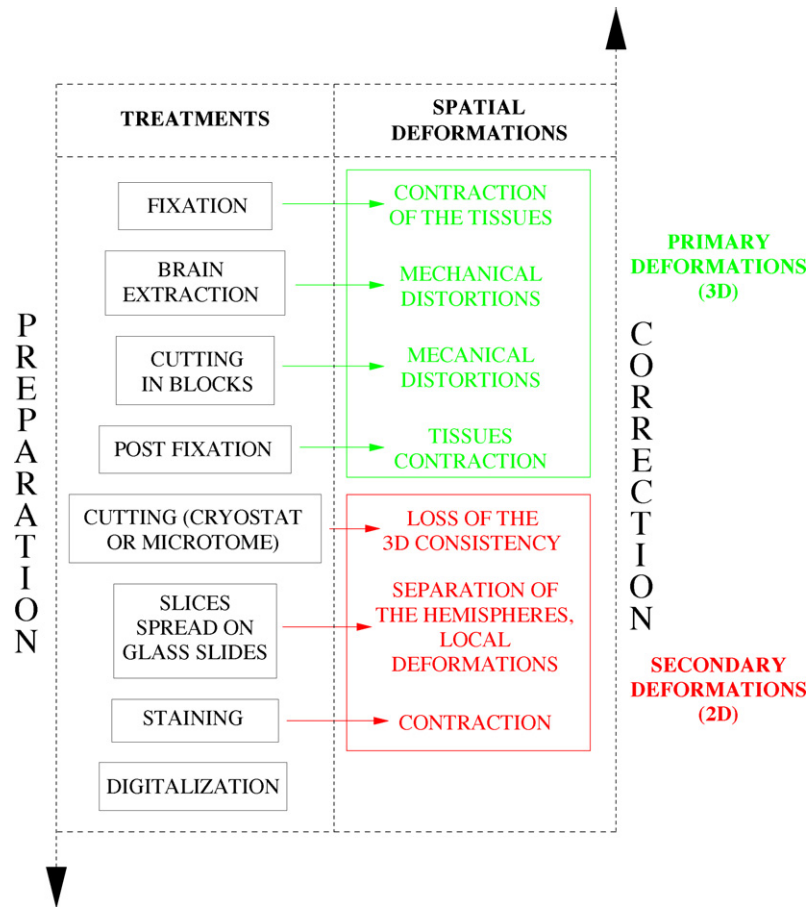
Fig. 1. The main steps of the preparation of cerebral histological slices and the associated deformations which have to be corrected to create an image comparable to the original brain. Note that the deformations of the biological material have to be corrected in the images in the reversed order compared to the one along with they occurred during the histological preparation.

structures). The anterior block contained the anterior part of the lenticular nucleus, the central block contained the whole thalamus, and the posterior block contained the remaining region posterior to the thalamus. For each baboon, a series of about 2200 sections in the coronal orientation was cut with a 40 μm slice thickness. One histological section out of 18 was extracted for this study so as to finally keep 121 sections with an associated slice spacing of 18 μm × 40 μm = 0.72 mm. These sections were mounted on glass slides and each section was then stained with both acetyl cholinesterase histochemistry and Nissl. They were digitized with a resolution of 800 dpi on a flat-bed *Image Scanner*^{TM} *I* (Amersham Biosciences) using transmission mode. We then chose to downsample the images to an isotropic in-plane resolution of 0.16 mm using bi-linear interpolation in order to ease the processing of the data while still having about five times higher in-plane resolution compared to the MRI data.

For both brains, blockface photographs were acquired during the sectioning process, using a digital camera HandyCam DCR-TRV30E (Sony Electronics Inc.) with high precision Carl Zeiss lens, 37 mm diameter. The photographs were taken at the end of the microtome sledge course, with the brain in the exact same position section after section. For each baboon brain, a series of about 2200 photographs were thus obtained with an in-plane resolution of 0.10 mm × 0.10 mm. Only the photographs corresponding to stained histological slices (one out of every 18) were kept and processed, leading to a series of 121 blockface photographs with the same slice spacing as the histological data (0.72 mm).

Fig. 1 summarizes the main deformations occurring during the histological preparation, and Fig. 2 gives an overview of our method to correct these deformations for the two baboon brains: the steps (A) and (B) are described below.

1.1. Blockface volume

For each brain, the photographs were first manually segmented (we explain in Section 3 why we did not perform automatic segmentation) using *Anatomist* software (Rivière et al., 2003) to separate the brain section from the embedding ice and set the background to zero. For each block, the series of photographs were stacked (no registration was necessary) to create a volume per block. To obtain the complete volume, the three already aligned photographic blocks were assembled together by applying a block-to-block 2D rigid registration estimated between the last slice of one block and the first slice of the following block. These two 2D rigid registrations used in our approach were performed with the blockmatching method as described in Ourselin et al. (2001).

Post mortem   In vivo

Stained histological slices   **Block face photographs**   **Anatomical T1 MRI**

2D hemi–rigid   3D rigid registration +
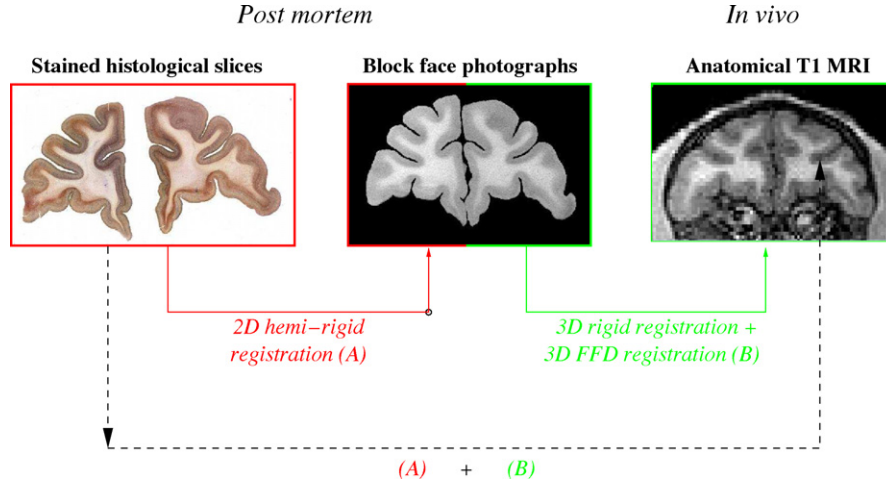registration (A)   3D FFD registration (B)

(A)   +   (B)

Fig. 2. The main steps of the *in-vivo/post-mortem* registration. Step (A) is correcting the 2D deformations (secondary deformations), and step (B) is correcting the 3D deformations (primary deformations) of the *post-mortem* brain to achieve the final matching with the MRI data.

1.2. Registration of histology with blockface photographs (step A)

First, the background of the histological stack of slices (processed as a 3D volume) was globally set to zero by thresholding, extraction of the largest 3D connected component and 3D morphological opening. After this pre-processing step, to perform the 2D *co-alignment* of the stained histological slices with the blockface photographs, we used the novel *hemi-rigid* method adapted to the registration of 2D slices with two hemispheres. The method consists of three steps:

- *Segmentation of the hemispheres*: the inter-hemispheric line, which divides the slice into two most symmetrical parts, is delineated. Prima et al. (2002) proposed an algorithm to determine the inter-hemispheric plane in 3D. We adapted this algorithm for our 2D slices. The idea consists initially in creating the symmetrical image of the original histological slice with respect to the vertical line of which equation is $x = \dim X/2$ (where $\dim X$ is the dimension of the image in the $\vec{x}$ horizontal direction and the origin is in the top left corner of the image). Then, the original image is rigidly registered to the symmetrical image: the rigid transformation obtained is noted (R, T), where R is the rotation matrix and T the translation vector. The "half" transformation is then estimated. This is the rigid transformation (r, t) verifying:

$$\forall x \in \Re^n, \quad Rx + T = r(rx + t) + t = r^2 x + (Id + r)t$$

In our case, $n = 2$. This formulation is also valid in 3D. As the decomposition of a rigid transformation Tr into a rotation matrix R and a translation vector T in the form $Tr(x) = Rx + T$ is unique, we have:

$$r^2 = R \tag{1}$$

$$t = (Id + r)^{-1} T \tag{2}$$

If the transformation (r, t) is applied to the vertical line $x = \dim X/2$, we then obtain the inter-hemispheric line (see Fig. 3(a)). This line divides the slice into at least two independent connected regions. To prevent from having a sub-part of one hemisphere in the wrong half image, the line is dilated with a radius of 1% of the horizontal size of the image. The two largest connected components are used as seeds (see Fig. 3(b)). A Voronoi like competitive dilation of the two seeds is then performed in the whole image, and the binary mask of the brain is applied to obtain the segmentation of each hemisphere (see Fig. 3(c)).

- *Estimation of one transformation per hemisphere*: the next step consisted in the estimation of an independent rigid transformation per hemisphere for registering each histological slice to the corresponding photograph. A global rigid registration for initialization is first applied (see Fig. 3(d)). The registration is based on the blockmatching displacement field and it uses a robust estimation based on the 50% least trimmed square method (Rousseeuw and Leroy, 1987). The rigid transformation estimated is mainly guided by one hemisphere, and the other one is being considered as an outlier region. A score of the quality of registration is calculated as the mean of the correlation coefficient of all the blocks in each hemisphere with the target image. The hemisphere with the higher score is named H_1, and the other one H_2. As H_1 is the best registered hemisphere, it is used to hide the corresponding hemisphere on the photograph. A new registration between H_2 and the masked photograph is then performed (see Fig. 3(e)). In this second pass, the "outlier" hemisphere H_2 by itself can be correctly registered to the correspondent hemisphere on the photograph, since the other one was hidden by H_1. Hiding the hemisphere which is not being registered at each step aims at limiting the risk of confusion in the search of corresponding regions (blockmatching) between hemispheres. This allows a better robustness of the method compared to a simultaneous estimation of the two rigid transformations followed by a
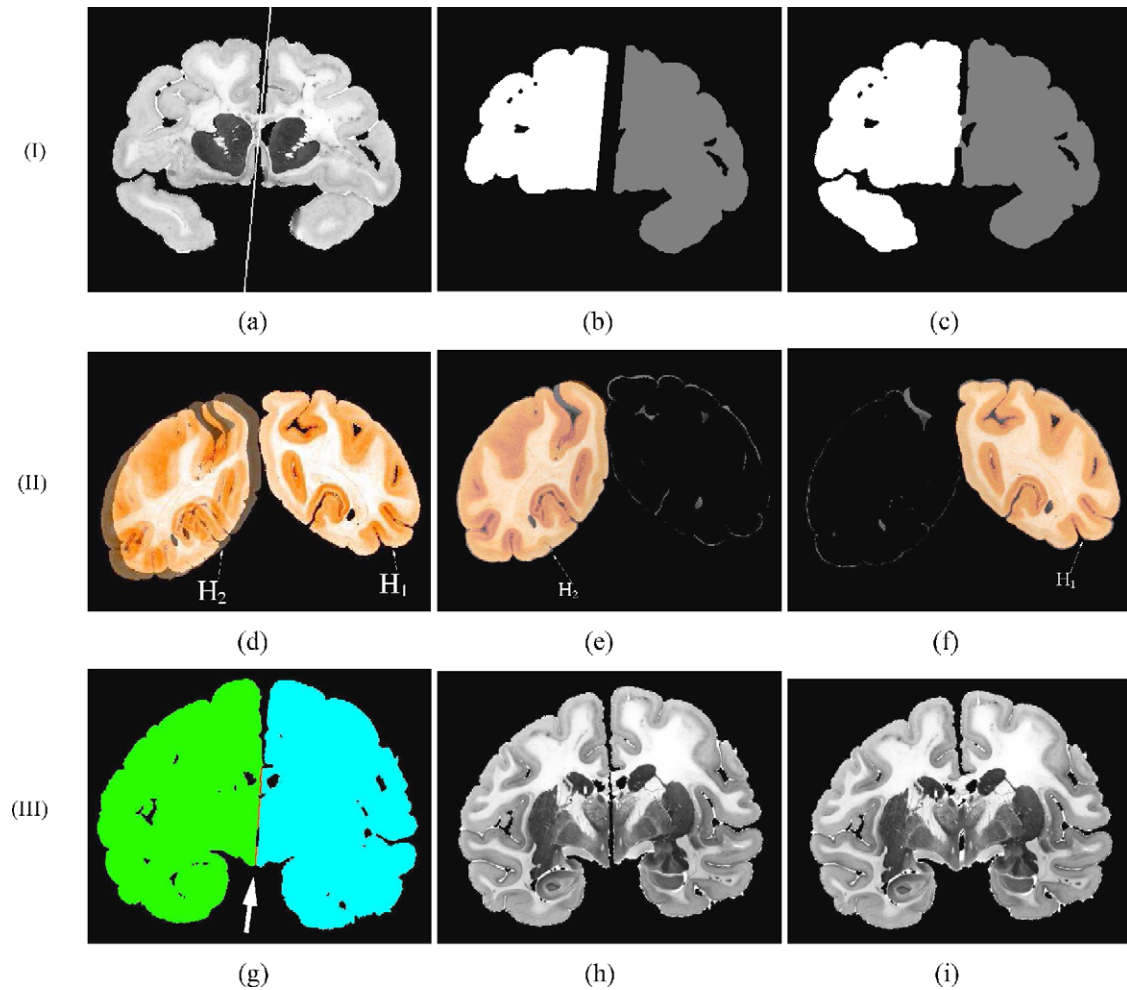
Fig. 3. The hemi-rigid method. (I) Automatic detection of the inter-hemispheric line (a), dilation of this line and conservation of the two biggest connected components (b) which are used as seeds for partitioning the slice into two hemispheres inside the binary mask (c). (II) Fusion images of a stained histological slice (false color orange) and its corresponding photograph. A global rigid registration is first realized (d), the better registered hemisphere H_1 is removed from both images allowing the correct registration of the other hemisphere H_2 (e). Finally, registration of H_1 is refined (f). (III) The frontier points between the two hemispheres are detected and paired ((g) white arrow). Each hemisphere is individually resampled using its own rigid transformation (h). A linear interpolation is realized between paired frontier points to fill up the gap (i). (For interpretation of the references to color in this figure legend, the reader is referred to the web version of the article.)

statistical analysis of the whole displacement field. The process is iterated once more, permuting the role of H_1 and H_2 to obtain a precise individual rigid transformation of each hemisphere (see Fig. 3(f)).

- *Resampling of the image*: for each hemisphere, the pixels which are connected (classical 2D 8-neighborhood connectivity) to at least one pixel from the other hemisphere are automatically detected; these pixels belong to the common frontier between the two hemispheres (see Fig. 3(g)). If the two hemispheres are two independent connected components, this set of points is void. All the detected points from each hemisphere are then paired with the closest point from the other hemisphere (the same point can be paired with multiple points). Each hemisphere is then resampled using its own rigid transformation previously estimated (see Fig. 3(h)). Hemisphere H_1 covers arbitrarily H_2 in case of superimposition. When the hemispheres are connected before registration, a continuous line is spatially traced between each couple of paired points of the frontier, and grey levels are linearly

interpolated along this line from the grey level of one frontier point to the grey level of the paired point. This simple interpolation allows the method to fill the void space resulting from the individual displacement of each hemisphere (see Fig. 3(i)).

All the histological slices were registered to the corresponding photograph using the hemi-rigid method, and then stacked to constitute the *histological volume* for each baboon brain. An inter-slice intensity normalization described in our work Dauguet et al. (2004) was then performed on both histological volumes (some slices appear imperfectly normalized because of a high intra-slice bias in our histological dataset, see paper for more details).

1.3. Registration of blockface volume with T1 MRI (step B)

For the registration of the blockface volume with the Tl MRI image, a first pre-processing step consisted in extracting the

brain from the rest of the head in the MRI using the anatomical pipeline of BrainVisa (Mangin et al., 1998). The resulting masked MRI image with only the brain was used for all the 3D registrations.

The blockface volume was first automatically rigidly registered to the MRI data (used as reference). The 3D transformation was estimated by optimization of the mutual information as similarity criterion as described in Viola and Wells (1997). From this rigid initialization, an elastic transformation of the blockface volume to the MRI was estimated using a Free Form Deformation (FFD) model (Rueckert et al., 1999; Mattes, 2000). Cubic B-splines driven by a grid of control points were used to model the deformation. The mutual information was chosen as the similarity criterion to maximize for the registration of the images. The optimizer used was a L-BFGS-B quasi-Newton algorithm (Byrd et al., 1995). The full resolution blockface volume was downsampled using median filter and tri-linear interpolation to a resolution consistent with the MRI data resolution. The resulting volume dimensions obtained were (in voxels) $106 \times 141 \times 87$ and $100 \times 129 \times 63$, respectively, for each baboon block-face volume before the elastic registration. A coarse to fine pyramidal based approach which consisted in increasing gradually the number of control points according to the three directions was chosen. According to the different volume dimensions, three levels were used for the two baboon images: from a $5 \times 6 \times 4$ regularly distributed grid for the first level, up to a $9 \times 10 \times 8$ regular grid for the last level, with an increment of two control points per level. The definition of the number of control points in the grid is aimed at preserving the distance between successive control points in the three directions in order to uniformly distribute the control points in the whole volume.

The quality of the final registration was evaluated by superimposing the external and internal borders of the MRI brain (extracted using Deriche filter, Deriche, 1987) onto the blockface volume. The FFD transformation estimated was also applied to a regular grid to determinate how the different regions were deformed. Moreover, the main sulci were semi-automatically extracted in both modalities (using the automatic human dedicated method described in Mangin et al., 1995). They were used to evaluate in 3D the quality of the registration in the cortical regions. Preliminary results for this step have been presented for one baboon in Delzescaux et al. (2003a).

1.4. Post-mortem histology to in-vivo MRI matching (A) + (B)

The 3D rigid and elastic transformations estimated between the blockface volume and the MRI data (step B) were directly applied to the full resolution histological volume previously obtained after "hemi-rigid" alignment (step A) for each baboon brain. We defined the resulting histological volume as the *Post-Mortem* Imaging (PMI) data. An evaluation of the elastic registration was performed visually by superimposing the transformed histological data on the MRI data for the two brains. The volume of the baboon brains were calculated on the histological data before (v_{histo}) and after the whole process of registration

(V_{histo}) and on the MRI data (reference volume V_{MRI}) to estimate a global shrinking coefficient ($s = v_{histo}/V_{MRI}$) and to compare the ability of the elastic transformation to recover the *in-vivo* geometry ($r = V_{histo}/V_{MRI}$).

All the software used in this study was implemented using the C++ AIMS libraries available in the BrainVisa/Anatomist package (Cointepas et al., 2001).

2. Results

Intermediary results were illustrated on one baboon. Final *in-vivo/post-mortem* matching were presented for the two baboons' brains.

For each baboon, three spatially consistent volumes were obtained after direct stacking of the series of photographs within the anterior, central and posterior blocks. The manual segmentation performed allowed the method to clearly process the brain in the images without background. No global deformation between the three different blocks was noted. A small part of the brain was inevitably lost between the blocks because the block faces were not perfectly flat. We quantified this loss by counting the lost sections (0.040 mm each). It was less than 18 tissue sections, which corresponded to less than one slice (0.72 mm) in the volume. The block-to-block rigid transformations visually achieved a decent assembly of the blockface volume. Whilst small discontinuities due to missing data could still be noticed at the intersections of blocks, the blockface volume showed a good spatial consistency (Fig. 4, column "Photographs").

The "hemi-rigid" co-alignment of the histological slices on the blockface slices was realized automatically with the same parameters for all the slices of both baboons (with the exception of 2 slices out of 121 with big distortions for each baboon). The histological slices and their corresponding photographs were similar in size, without any noticeable scale factor. Fig. 4, column "Histology", demonstrates the 3D spatial consistency of the histological volume after the "hemi-rigid" alignment onto the blockface volume. The mounting on glass slides step induced tearings, foldings, and lost parts for some sections. Therefore, the histological volume presented more artefacts than the blockface volume. They can be noticed as small black regions along a slice on the axial and sagittal views.

The hemispheres in the blockface photographs had a natural consistent location from one slice to another. After the hemi-rigid alignment, the geometry of the histological volume was similar to the blockface one, as demonstrated on the checkerboard composite of the 2 volumes (Fig. 4, column "Checkerboard"). Yet, the histology presented a dramatically improved quality of contrast and definition of the structures compared to the blockface photographs. The cerebellum was manually removed from the blockface photographs and the histological slices, since it is a complex region which was divided in multiple parts after cutting. Moreover, it was of no interest in our study.

The use of our novel "hemi-rigid" registration to align the histological slices onto the blockface slices proved to be more accurate than the rigid registration, as shown in Fig. 5. The main
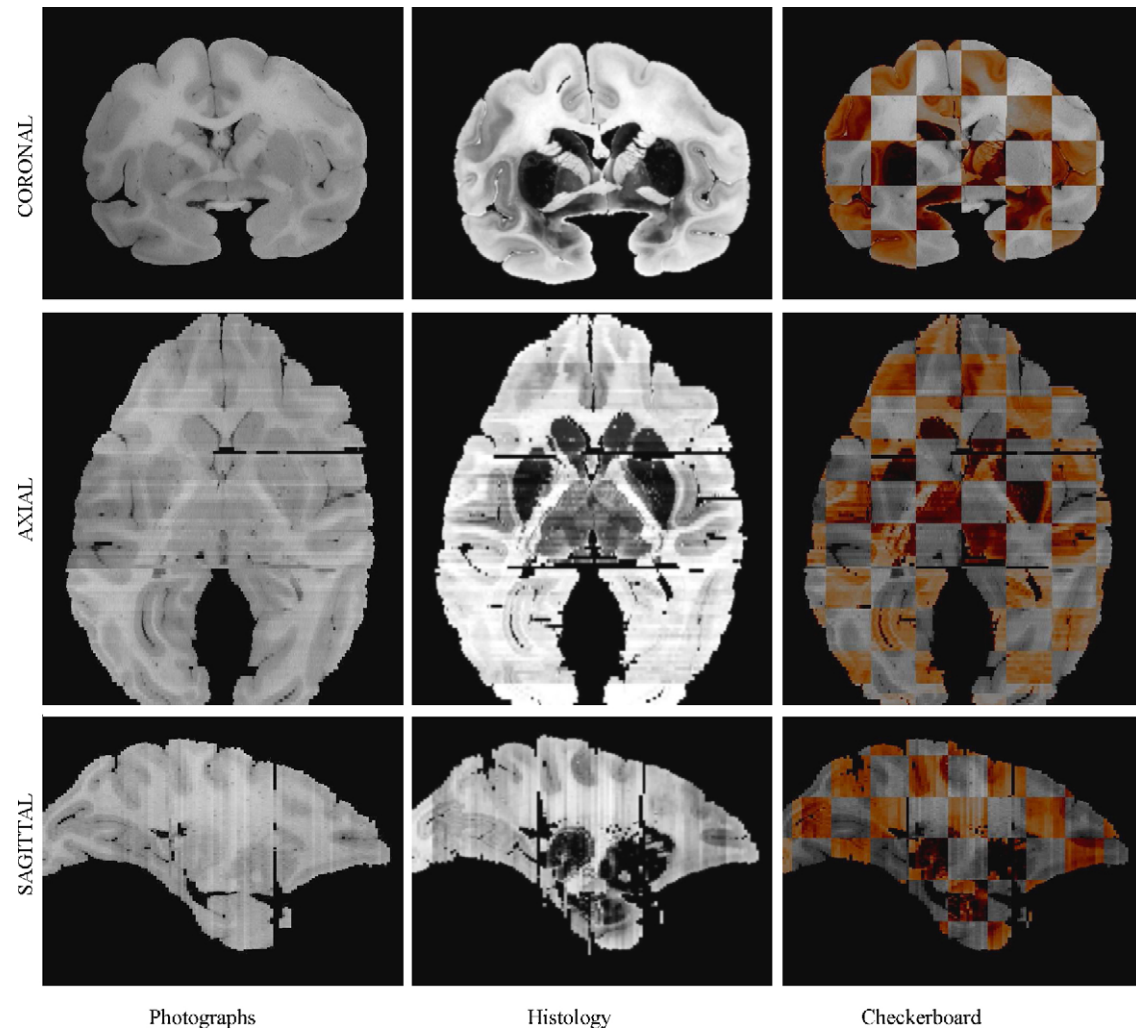
Fig. 4. Column "Photographs ": the blockface volume obtained after segmentation of the brain and assembly of the three aligned blocks. Column "Histology": reconstructed histological volume using hemi-rigid co-alignment strategy. Column "Checkerboard": the blockface volume in false orange color is presented together with the MRI data in checkerboard mode. All results are presented for the same baboon in coronal (cutting orientation), axial and sagittal views as indicated. (For interpretation of the references to color in this figure legend, the reader is referred to the web version of the article.)
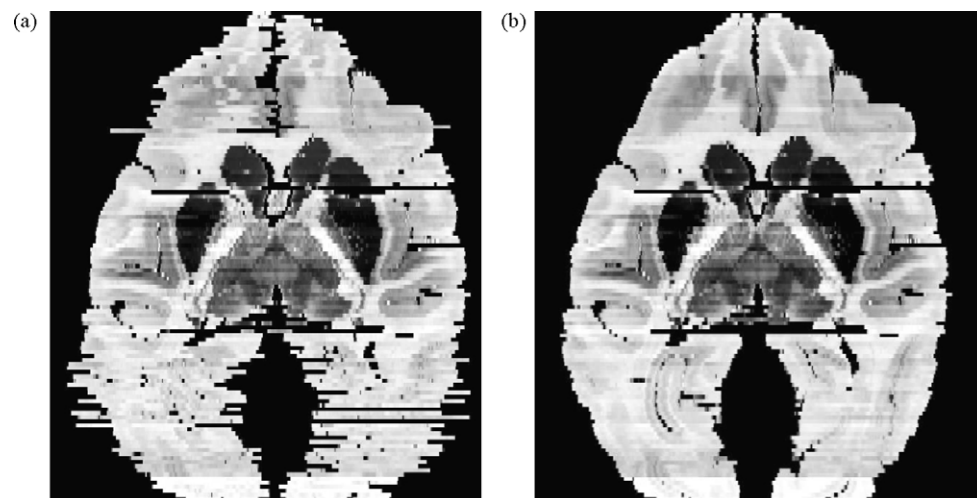

Fig. 5. Comparison of the 3D spatial consistency obtained for the reconstructed histological volume using the classical rigid registration (a) and using the hemi-rigid registration method (b) in axial view.
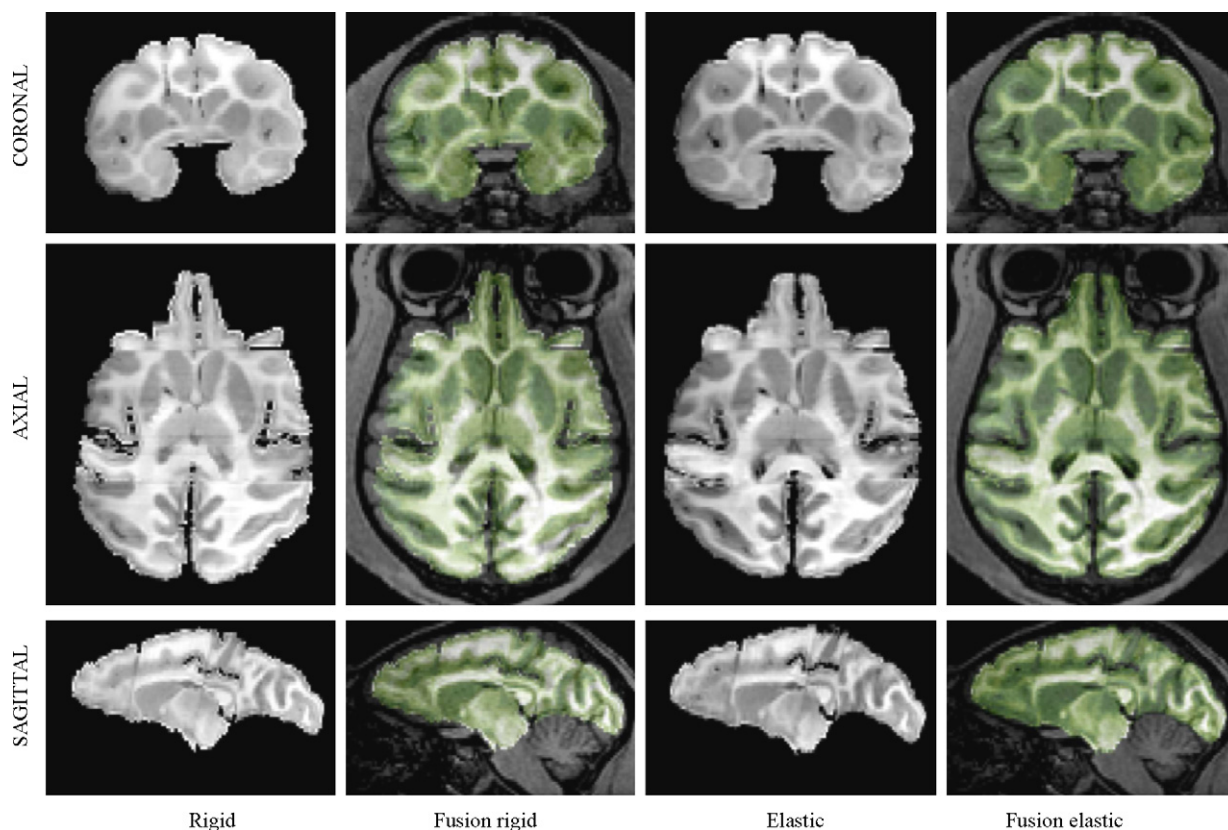
Fig. 6. 3D registration of the blockface volume with the MRI data. Column "Rigid": 3D rigid initialization, blockface volume alone. Column "Fusion rigid": same volume superimposed with the MRI data. Column "Elastic": correction of the deformations of the blockface volume using FFD alone. Column "Fusion elastic": same volume superimposed with the MRI data. The blockface volume appears in false color green in fusion images. All results are presented in coronal, axial and sagittal views as indicated.

differences can be noticed in the anterior and posterior part of the brain, where the hemispheres were not connected. Contrary to the photographs, the relative position of the two hemispheres in the histological slices was lost while they were spread on glass slides. Consequently, the simple global rigid transformation did not properly align each slice on its corresponding photograph, leading to a poorly consistent 3D reconstruction (a). Contrarily, the use of the hemi-rigid strategy to reconstruct the histological volume (b) performed an improved alignment, with a good 3D spatial consistency. Although the local deformations (foldings, tearings and displacements of gyri) were not corrected, we could see a dramatic improvement of the alignment with the hemi-rigid method. This observation demonstrated that the independent motion of each hemisphere was the most important deformation to correct for the 3D reconstruction of the histological volume.

Both the rigid and elastic transformations between the segmented blockface volume and the MRI were estimated on the masked brains. However, the positioning of the histological brain relatively to the eyes, the cerebellum and the skull were appreciated on the MRI image presented with the whole head (Fig. 6). The preliminary rigid registration (columns "Rigid" and "Fusion rigid") provided a fair matching of the internal structures of the brain (basal ganglia). However, important misregistrations were remaining particularly in the cortical parts as could be clearly seen in the superimposition images. The

estimation of the elastic transformation using the FFD method definitely improved the quality of the registration between the blockface volume and the MRI (columns "Elastic" and "Fusion elastic") compared to the rigid transformation, particularly in the peripheral region of the brain. The elastic transformation was mainly an inflation to correct the global shrinkage of the *post-mortem* brain compared to the MRI data. Some misalignments can still be seen in the left and right temporal pole and for the sylvian/insular region on the right side in the axial views, as well as for the parietal area in the sagittal view, but overall the matching is good.

More precisely, the main internal and external MRI contours were compared to the blockface volume after rigid registration and after the correction of the deformations using the FFD method. As shown in Fig. 7, column "Rigid" and "Elastic", the matching of all the structures delineated was improved by the elastic transformation. The FFD deformation estimated was smooth, realistic and with no topological distortions (Fig. 7, column "deformation grid"). Moreover, as one could expect, the displacements were rather symmetrical and the high deformations were mostly peripheral.

The 3D sulci extraction on both the MRI data and the blockface volume for the left and right hemispheres were very similar (Fig. 8). This similarity in shape assessed the realistic 3D consistency of the reconstructed blockface volume compared to the *per se* 3D consistent MRI data. However, a non-satisfactory
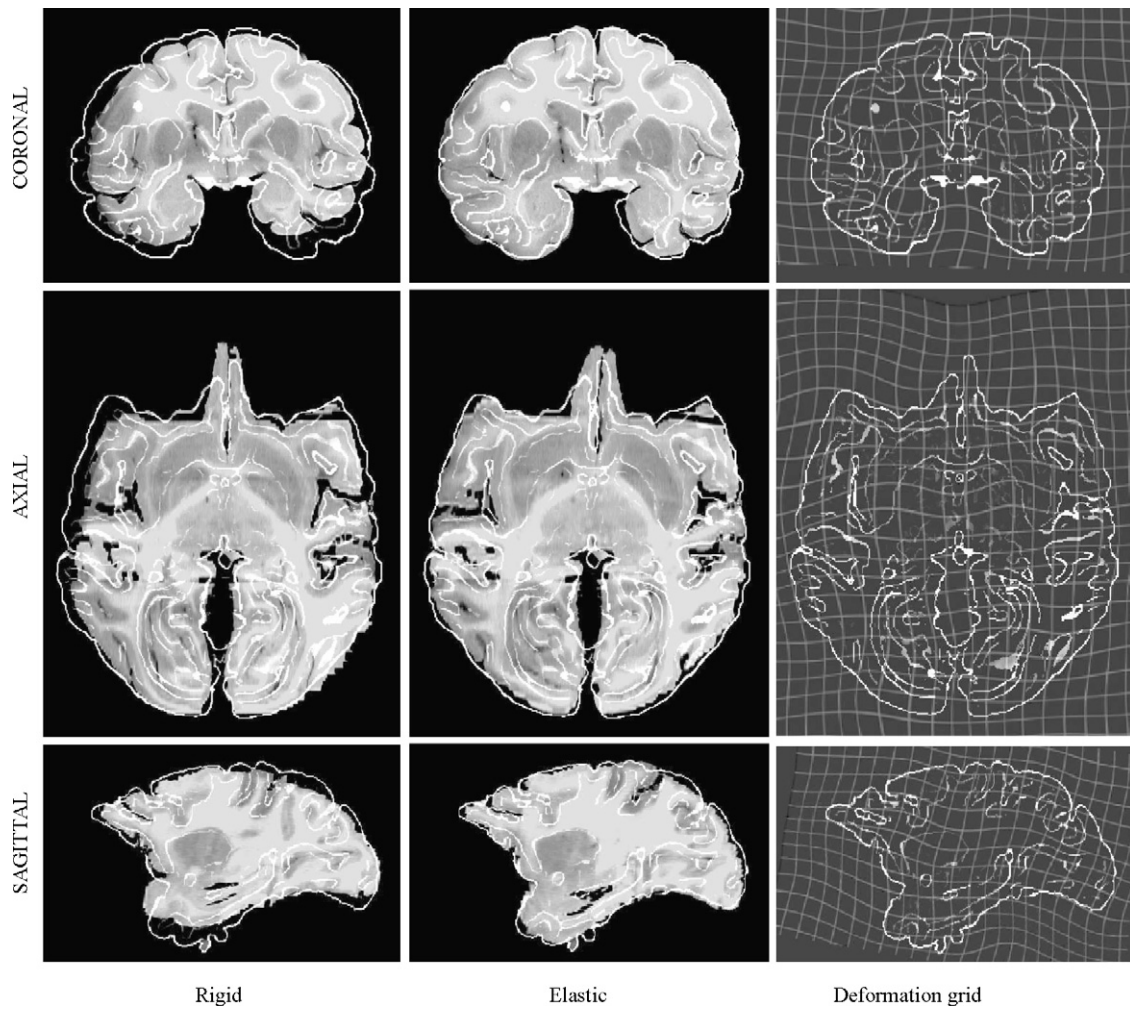
Fig. 7. Main contours of the MRI data of one baboon brain superimposed on the blockface volume before and after the FFD elastic correction, in coronal, axial and sagittal views. Last column: same MRI contours superimposed on a regular grid deformed by the FFD transformation.
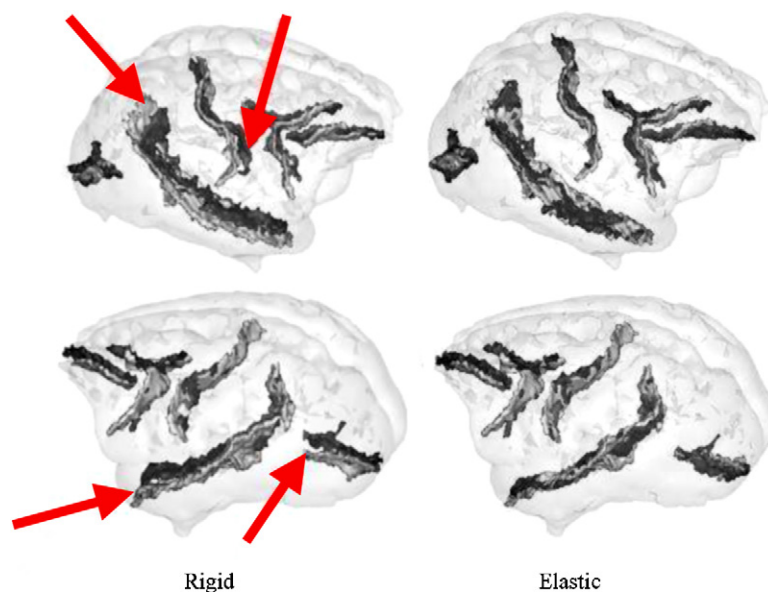

Fig. 8. Surface rendering of the right (top) and left (bottom) hemisphere of one baboon brain with the main sulci extracted on the MRI (dark grey) and on the blockface volume (light grey) before and after elastic correction was applied. The arrows indicate the main mismatchings before elastic correction.
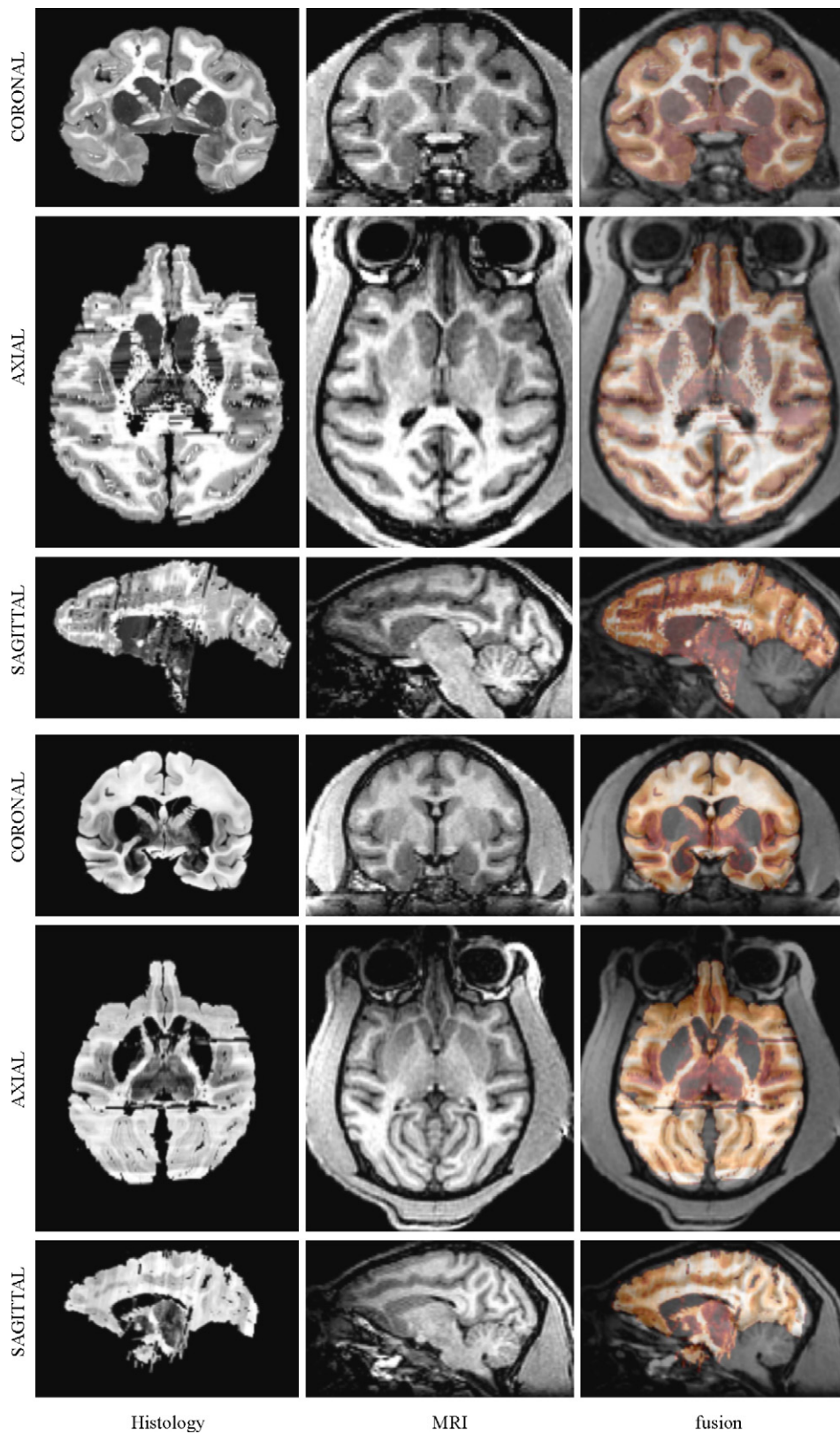
Fig. 9. Final matching of the series of stained histological slices (*post-mortem* data) with the MRI image (*in-vivo* data) for the two baboons (top and bottom). The histological volume appears in false color orange in the fusion images with the MRI data. All results are presented in coronal, axial and sagittal views as indicated.

matching of sulci was obtained after rigid registration (locations indicated by the arrows, column "Rigid"). After the elastic correction was applied, the matching of some sulci was improved both on the right and left hemispheres (sulci pointed to by arrows in column "Rigid", which are better matched in column "elastic").

As previously shown, the histological and blockface volume had a similar geometry after hemi-rigid alignment. Therefore, the final results of the elastic registration between the histological volume and the MRI (Fig. 9) were comparable to those presented for the blockface volume (Fig. 6). Whilst some small differences between the 2 volumes were noticed, the transformed histological volume was realistic and the global shrinkage was corrected. Observations performed in the three orientations confirmed a uniform good matching of internal and external structures with the MRI in all the regions of the brain. The elastic transformation estimated on the blockface volume thus effectively corrected deformations of different nature and amplitude of the histological volume without spurious distortion. It can be noted in the sagittal views, the oblique orientation of the histological slices which deformed to match the MRI data. Many details of the brain anatomy became visible with the contrast and resolution of the histological volume. In particular, the internal capsule in the striatum could be distinguished on the histology, but is barely visible on the MRI data alone.

The volumes of the brains computed on the MRI data of the two baboons, respectively 132 and 143 cm^3, were consistent with the literature (Rilling and Insel, 1999, 143 ± 16 cm^3). The volume of the histological image estimated before the elastic registration (113 and 122 cm^3) presented a global 15% shrinkage compared to the MRI data for the two baboon brains processed. This value was slightly over estimated since, as we discussed, some small parts were missing in the histological image, particularly at the interfaces of the blocks. Yet, this result gave an appreciation of the extent of the global histological deformations. It confirmed the existence of major deformations between *post-mortem* and *in-vivo* data, mainly due to the dehydration of the tissues during extraction, fixation and staining processes. After the elastic transformation was applied, the volumes of both corrected histological data (135 and 138 cm^3) and the target MRI data were similar, with a difference of 2% and 3%, respectively, for each baboon brain. The volumes and shrinkage ratios computed were summarized in Table 1.

Table 1
Volumes estimated for the whole brain in the original *in-vivo* geometry represented by the MRI data, and volume and shrinkage ratios of the whole brain estimated for the histological *post-mortem* volume before and after correction of deformation using FFD

	Volume A (cm^3)	Volume B (cm^3)	Shrinkage ratio A	Shrinkage ratio B
MRI	$V_{MRI} = 132$	$V_{MRI} = 143$	–	–
Histology (before FFD)	$v_{histo} = 113$	$v_{histo} = 122$	0.85	0.85
Histology (after FFD)	$V_{Histo} = 135$	$V_{Histo} = 138$	1.02	0.97

Results are presented for the two baboons called "A" and "B".

3. Discussion

3.1. Interest of the blockface volume as an intermediary modality

As described in the results section, the blockface volume presented fewer artifacts (displacement of gyri, torn or missing parts, foldings) than the histological one. The blockface volume was obtained by direct stacking since the method of acquisition of the photographs guaranteed a direct alignment of all the images inside each individual block. Moreover, despite some missing slices, the blocks assembly could be resolved leading to a 3D consistent blockface volume. Since each histological slice was registered to its corresponding blockface photograph, the 3D curvature of the *post-mortem* brain was preserved and the "banana problem" (Streicher et al., 1997) was thus avoided. Concerning the manual segmentation of the brain in the blockface photographs to remove the background (mainly embedding ice), it seemed too difficult to robustly automate the processing despite our efforts, since the contrast between ice and tissue was very low. This step is time consuming indeed. We have since tested some new dyes for the ice in order to overcome this difficulty and the results are extremely promising: some successful ice segmentations have been obtained automatically.

Nevertheless, the blockface photographs remained an intermediary modality used mainly for methodology purposes since blockface photographs were not stained and could only be acquired remotely with a camera in reflection mode. Consequently, the resolution for analysis and the contrast between specific tissues were limited compared to the histological sections. Recent works (Annese et al., 2006) overcame some of these limitations with the use of a special dye injected *in-vivo* which produces a staining of the *post-mortem* brain that enhances blockface photograph contrast. Yet, contrary to histological slices, it is still impossible to stain with a different coloration multiple sub-series of block face photographs covering the whole brain, and to scan them at a very high resolution using a microscope.

3.2. The hemi-rigid co-alignment

Even though the brain is fairly symmetrical, it is essential for the biomedical community to consider, in particular studies, both hemispheres for 3D reconstruction and then matching with *in-vivo* data. Indeed, the anatomical and functional asymmetry of the brain, primate's brain in particular, have been studied (Sastre-Janer et al., 1998; Toga and Thompson, 2003), but they are still imperfectly known. The asymmetry studies performed using *in-vivo* imaging techniques like MRI are limited because of the relatively limited resolution and contrast available even on the most recent and powerful biomedical scanners. Conversely, the precision of analysis provided by the stained histological slices enables one to detect subtle differences between hemispheres (see, for instance, the works of Bürgel et al., 1999, on white matter connectivity). Dealing with both hemispheres for 3D histological reconstruction is thus a relevant issue, which

appears to be particularly suitable for asymmetry studies (e.g. Rademacher et al., 2001).

The direct use of affine alignment (Hibbard and Hawkins, 1988; Andreasen et al., 1992; Zhao et al., 1993; Goldszal et al., 1995; Schormann et al., 1995; Rangarajan et al., 1997; Cohen et al., 1998; Ourselin et al., 2001; Bardinet et al., 2002; Malandain et al., 2004) was not adapted for the 3D reconstruction of a whole primate brain from histological slices because of the separate motion of the hemispheres. While 2D elastic transformations (Kim et al., 1997; Mega et al., 1997; Schormann and Zilles, 1998; Chakravarty et al., 2006) can ultimately correct local deformations, their high number of degrees of freedom made them too flexible to only recover the independent, rigid displacement of separated hemispheres without introducing undesired, non-rigid deformations. Moreover, it is usually more challenging to perform non-linear registration with the same parameters for a large series of slices without errors, although some of the authors previously cited have used the same set of parameters for the processing of their data. As for the locally affine transformations proposed by Pitiot et al. (2006) or Arsigny et al. (2005), they seem suitable for the correction of local deformations of histological material. However, while these methods can deal with more than two piecewise regions and thus have the flexibility to register sub-regions more precisely, they do not use any biological *a priori* knowledge and consequently it is not guaranteed the correction they perform is anatomically pertinent.

The hemi-rigid method we proposed for the co-alignment of stained histological slices with the corresponding blockface photographs proved to correctly solve the problem of automatically estimating individual rigid transformations for separated hemispheres. While some local misalignments could benefit from additional non-linear corrections, our method provides the same advantages as the rigid transformation, since robustness and integrity of the data were preserved. The interpolation used for some slices to fill the small void regions resulted from the individual resampling of each hemisphere guaranteed to keep entirely the original information included in the original section.

The robustness of our method was adapted to the automatic processing of large series of slices including both hemispheres. The blockmatching technique was used (Ourselin et al., 2001) for the estimation of the rigid transformation for each hemisphere. It was particularly well adapted for the registration of histological slices since it used a local approach and a robust estimation scheme. It could therefore cope with the missing parts, tearings, and artifacts in a more robust way than could global estimation registrations do. The correlation coefficient was chosen as similarity criterion: it is adapted for affine relations between intensities. This approximation of an affine relation between intensity distributions was locally verified between the grey levels of the stained histological slices and the grey levels of the blockface photographs since the regions (blocks) were sufficiently small.

The hemi-rigid transformation could be generalized to any type of transformations (affine or non-linear) and to more than two independent regions provided that they are segmented. The choice to use in this work rigid transformations for each hemisphere was made to better preserve the integrity of the biological

data before the elastic registration. We also chose to limit the parcellation of the slice to the segmentation of the two hemispheres for robustness reasons and because their relative displacement constituted by far the main secondary deformation that had to be corrected. For many histological slices, the hemispheres were slightly connected but had moved individually: this justified our methodological choice to perform the hemi-rigid registration for all the slices, including the ones with connected hemispheres.

The secondary deformations listed in Fig. 1 can be re-ranked with respect to the magnitude of the deformation, given here in the decreasing order:

(1) the global loss of the 3D spatial consistency due to cutting;
(2) the independent spreading of the hemispheres of the sections on glass slides;
(3) the remaining 2D local deformations (including displacement of gyri in each hemisphere, contraction, tearing, overlapping, crumpling . . .).

Commonly, the item 1 (global loss of the 3D spatial consistency of the histological data) is corrected simply by a classical affine alignment as we have described in the introduction. In this study, we proposed to correct both items 1 and 2 using our hemi-rigid method; item 3 is not addressed in this work. We intended to favor robustness and simplicity in our protocol. The results demonstrated that our method provided satisfactory reconstructed histological volumes (see Fig. 4).

The hemi-rigid method uses some *a priori* biological knowledge on the image to process, since it performs the segmentation of each hemisphere before the registration. To go further in the correction of the secondary deformations (item 3), additional *a priori* biological knowledge is to be introduced to prevent performing non-realistic deformations, which has not yet been done to the best of our knowledge. Some other methods already mentioned could be used to go further in the correction of these types of secondary deformations, even though they were only tested on one hemisphere. The method proposed by Pitiot et al. (2006) can deal with the displacements of gyri. As for the last type of deformations, we can suggest the works of Arsigny et al. (2005) proposing to control the degrees of freedom of the non-linear transformation applied, which could be suitable for some local corrections. Chakravarty et al. (2006) also proposed to use a warping method to histological material to improve the alignment of slices. Sensibility to the parameters of the 2D non-linear transformations should be noted to avoid spurious and non-realistic deformations.

3.3. The free form deformation

We chose to use the FFD method to correct the primary deformations (which are 3D deformations, see Fig. 1). This method was originally dedicated to the correction of breast deformations (Rueckert et al., 1999) and it was also used to successfully correct the deformations for thorax respiration motions between Positon Emission Tomography (PET) and Computer Tomography (CT) scan (Mattes et al., 2003; Delzescaux et al., 2003b). The method is generic and it offers a good control on the flexibility of the

deformation controlled by the grid chosen. The coarse-to-fine approach we chose assured a progressive correction, and robustness was obtained because of the quite limited final degrees of freedom, which avoided wrong warping in the case of histological distortions. A trade-off concerning the number of control points used was found to allow an accurate registration of the different regions and to avoid spurious deformations.

We chose to apply the 3D rigid and elastic FFD-based transformations estimated between the blockface volume and the MRI data to the reconstructed histological volume. The elastic transformations like FFD are in general more sensitive to artifacts, such as tearing or missing parts because of the high number of degrees of freedom compared to linear transformations. Consequently, we used the blockface volume to estimate the elastic transformation with the MRI data since, among *post-mortem* modalities, it suffered fewer artifacts than the histological volume. Tests of estimation of the elastic FFD transformation directly between the histological volume and the MRI data resulted in both less accurate and less robust results.

4. Conclusion

The protocol described in this paper offers a framework to match a series of stained histological slices with the MRI scan of primate brains. Two complete baboon brains were first reconstructed from stained histological slices and then brought back to their original *in-vivo* geometry. The final reconstructed stained histological volumes were presented for the whole brain (including both hemispheres) of two baboons, in high resolution with no smoothing, in coronal, axial and sagittal orientation, alone and superimposed with the corresponding MRI.

Three important properties of the final histological volume obtained were achieved by using our protocol: it was (1) spatially 3D consistent, (2) brought back to the *in-vivo* geometry, and (3) representing the whole brain including both hemispheres. This final volume verifying these three properties can thus be considered as a 3D biomedical modality: the *Post-Mortem* Imaging (PMI). The *post-mortem* modality provides high resolution information in the same 3D geometry as *in-vivo* imaging (as shown in Fig. 10). Additionally, our protocol does not rely on any specificity of the baboon brain and it can be applied to most primate brains and, more particularly, to human brains.

PMI offers new opportunities for biomedical studies involving histology. Accurate 3D atlases representing the whole brain in the *in-vivo* geometry can be created based on the high resolution histological information. It also enables the validation and testing of imaging techniques processed on *in-vivo* data (fMRI, DTI, and PET) by the confrontation with the gold standard embodied by the information derived from the actual tissues.

In conclusion, this work demonstrates a method which bridges the gap between fundamental biological research relying on *post-mortem* microscopic material analysis and clinical applications relying on *in-vivo* macroscopic medical images analysis.
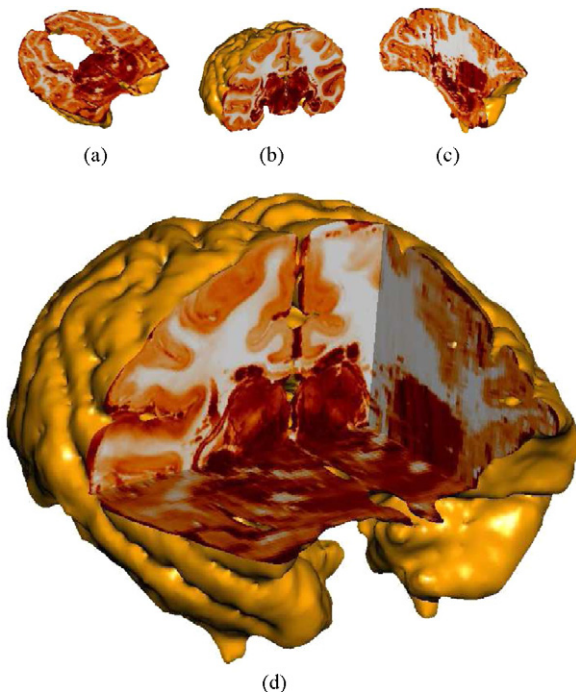
Acknowledgments

Fig. 10. The *post-mortem* Imaging (PMI) data for one baboon included in the surface rendering of the MRI data with different axial (a), coronal (b), sagittal (c) and multiple (d) clipping plans. The PMI modality obtained is spatially 3D consistent, is in the MRI geometry and represents the whole brain.

References

Andreasen A, Drewes A, Assentoft J, Larsen N. Computer-assisted alignment of standard serial sections without use of artificial landmarks. a practical approach to the utilization of incomplete information in 3-D reconstruction of the hippocampal region. J Neurosci Methods 1992;45:199–207.

Annese J, Sforza D, Dubach M, Bowden D, Toga A. Postmortem high-resolution 3-dimensional imaging of the primate brain: blockface imaging of perfusion stained tissue. Neuro Image 2006;30:61–9.

Arsigny V, Pennec X, Ayache N. Polyrigid and polyaffine transformations: a novel geometrical tool to deal with non-rigid deformations—application to the registration of histological slices. Med Image Anal 2005;9:507–23.

Ashburner J, Friston K. Spatial transformation of images. In: Frackowiak R, Friston K, Frith C, Dolan R, Mazziotta J, editors. Human brain function. USA: Academic Press; 1997. p. 43–58.

Bardinet E, Ourselin S, Dormont D, Malandain G, Tandé D, Parain K, et al. Co-registration of histological, optical and MR data of the human brain. In: Dohi T, Kikinis R, editors. Medical image computing and computer-assisted intervention (MICCAI'02). Tokyo: Springer; 2002. p. 548–55.

Bürgel U, Schormann T, Schleicher A, Zilles K. Mapping of histologically identified long fiber tracts in human cerebral hemispheres to the mri volume of a reference brain: position and spatial variability of the optic radiation. Neuro Image 1999;10:489–99.

Byrd R, Lu P, Nocedal J, Zhu C. A limited memory algorithm for bound constrained optimization. SIAM J Sci Comp 1995;16:1190–208.

Cachier P, Bardinet E, Dormont D, Pennec X, Ayache N. Iconic feature based nonrigid registration: The PASHA algorithm. CVIU—Special Issue on Nonrigid Registration, 2003;89:272–98.

Chakravarty M, Bertrand G, Hodge C, Sadikot A, Collins D. The creation of a brain atlas for image guided neurosurgery using serial histological data. Neuroimage 2006;30:359–76.

Christensen G, Joshi S, Miller M. Volumetric transformation of brain anatomy. IEEE Trans Med Imaging 1997;16:864–77.

Christensen G. Consistent linear-elastic transformations for image matching. Information processing in medical imaging, vol. 1613. Springer-Verlag; 1999. p. 224–37.

Clatz O, Delingette H, Talos IF, Golby AJ, Kikinis R, Jolesz FA, et al. Robust non-rigid registration to capture brain shift from intra-operative MRI. IEEE Trans Med Imaging 2005;24:1417–27.

Cohen F, Yang Z, Huang Z, Nissanov J. Automatic matching of homologous histological sections. IEEE Trans Biomed Eng 1998;45:642–9.

Cointepas Y, Mangin JF, Garnero L, Poline JB, Benali H. BrainVISA: software platform for visualization and analysis of multi-modality brain data. In: Proceedings of 7th HBM; 2001. p. S98.

Collins D, Evans A. Toga A, editor. Animal: automatic non-linear image matching and anatomical labeling. Academic Press; 1998.

Dauguet J, Dubois A, Hérard AS, Besret L, Bonvento G, Syrota A, et al. An automated and robust protocol to reconstruct 3D volume from histological sections: application to an activation study in rat brain. Toronto: The Society of Nuclear Medicine (SNM); 2005.

Dauguet J, Mangin JF, Delzescaux T, Frouin V. Robust inter-slice intensity normalization using histogram scale-space analysis. In: Barillot C, Haynor DR, Hellier P, editors. Medical image computing and computer-assisted intervention (MICCAI 2004), vol. 3216. Saint-Malot, France: Springer Verlag; 2004. p. 242–9.

Davatzikos C. Spatial transformation and registration of brain images using elastically deformable models. Comp Vis Image Understanding: CVIU 1997;66:207–22.

Delzescaux T, Dauguet J, Condé F, Maroy R, Frouin V. Using 3D non rigid FFD-based method to register *post-mortem* 3D histological data and in vivo MRI of a baboon brain. In: Ellis RE, Peters TM, editors. Medical image computing and computer-assisted intervention (MICCAI 2003), vol. 2879. Montreal, Canada: Springer Verlag; 2003a. p. 965–6.

Delzescaux T, Foehrenbach H, Frouin V. A performance study for whole-body helicoidal CT/PET-FDG a posteriori registration using rigid and non-rigid FFD-based methods. In: Proceedings of society of nuclear medicine (SNM); 2003b.

Deriche R. Separable recursive filtering for efficient multi-scale edge detection. In: Proceeding international workshop on machine vision and machine intelligence; 1987. p. 18–23.

Drouot X, Oshino S, Besret L, Jarraya B, Kishima H, Rémy P, et al. Functional recovery in a primate model of Parkinson's disease following motor cortex stimulation. Neuron 2004;44:769–78.

Friston K, Ashburner J, Frith C, Poline J, Heather JD, Frackowiak R. Spatial registration and normalization of images. Hum Brain Map 1995;2:165–89.

Gardella D, Hatton W, Rind H, Rosen G, von Bartheld C. Differential tissue shrinkage and compression in the *z*-axis: implications for optical disector counting in vibratome-, plastic- and cryosections. J Neurosci Methods 2003;124:45–9.

Goldszal A, Tretiak O, Hand P, Bhasin S, McEachron D. Three-dimensional reconstruction of activated columns from 2-[14*c*]deoxy-image-glucose data. Neuroimage 1995;2:9–20.

Hibbard L, Hawkins R. Objective image alignment for three-dimensional reconstruction of digital autoradiograms. J Neurosci Methods 1988;26:55–74.

Kim B, Boes J, Frey K, Meyer C. Mutual information for automated unwarping of rat brain autoradiographs. Neuro Image 1997;5:31–40.

Maes F, Collignon A, Vandermeulen D, Marchal G, Suetens P. Multimodality image registration by maximization of mutual information. IEEE Trans Med Imaging 1997;16:187–98.

Maintz J, Viergever M. A survey of medical image registration. Med Image Anal 1998;2:1–36.

Malandain G, Bardinet E, Nelissen K, Vanduffel W. Fusion of autoradiographs with an MR volume using 2-D and 3-D linear transformations. Neuro Image 2004;23:111–27.

Mangin JF, Coulon O, Frouin V. Robust brain segmentation using histogram scale-space analysis and mathematical morphology. In: Proceedings of the 1st MICCAI, 1496. Boston: Springer Verlag; 1998. p. 1230–41.

Mangin JF, Frouin V, Bloch I, Régis J, López-Krahe J. From 3D magnetic resonance images to structural representations of the cortex topography using topology preserving deformations. J Math Imaging Vis 1995;5:297–318.

Mattes D. Automatic multimodality image registration with deformations. Technical report, Thesis for the degree of MS in Electrical Eng. Ph.D. diss., Seattle: University of Washington Medical Center; 2000.

Mattes D, Haynor D, Vesselle H, Lewellen T, Eubank W. PET-CT image registration in the chest using free-form deformations. IEEE Trans Med Imaging 2003;22:120–8.

Mega M, Chen S, Thompson P, Woods R, Karaca T, Tiwari A, et al. Mapping histology to metabolism: coregistration of stained whole-brain sections to premortem PET in aAlzheimer's disease. NeuroImage 1997;5:147–53.

Ourselin S, Roche A, Subsol G, Pennec X, Ayache N. Reconstructing a 3D structure from serial histological sections. Image Vis Comp 2001;19:25–31.

Pitiot A, Bardinet E, Thompson P, Malandain G. Piecewise affine registration of biological images for volume reconstruction. Med Image Anal 2006;10:465–83.

Prima S, Ourselin S, Ayache N. Computation of the mid-sagittal plane in 3d brain images. IEEE Tran Med Imaging 2002;21:122–38.

Rademacher J, Bürgel U, Geyer S, Schormann T, Schleicher A, Freund HJ, et al. Variability and asymmetry in the human precentral motor system: a cytoarchitectonic and myeloarchitectonic brain mapping study. Brain 2001;124:2232–58.

Rangarajan A, Chui H, Mjolsness E, Pappu S, Davachi L, Goldman-Rakic P, et al. A robust point-matching algorithm for autoradiograph alignment. Med Image Anal 1997;1:379–98.

Rilling J, Insel T. Differential expansion of neural projection systems in primate brain evolution. NeuroReport 1999;10:1453–9.

Rivière D, Regis J, Cointepas Y, Papadopoulos-Orfanos D, Cachia A, Mangin JF. A freely available anatomist/brainvisa package for structural morphometry of the cortical sulci. Hum Brain Map 2003;934.

Rousseeuw P, Leroy A. Robust regression and outlier detection. In: Series in applied probability and statistics. New York: Wiley-Interscience; 1987.

Rueckert D, Sonoda LI, Hayes C, Hill DL, Leach MO, Hawkes DJ. Non-rigid registration using free-form deformations: application to breast MR images. IEEE Trans Med Imaging 1999;18:712–21.

Sastre-Janer FA, Thivard L, Belin P, Masure MC, Lehericy S, Frouin V, et al. Human central sulcus asymmetry and handedness: three-dimensional anatomical and functional imaging studies. J Cogn Neurosci 1998:91.

Schormann T, Dabringhaus A, Zilles K. Statistics of deformations in histology and application to improved alignment with MRI. IEEE Trans Med Imaging 1995;14:25–35.

Schormann T, Zilles K. Three-dimensional linear and nonlinear transformations: an integration of light microscopical and mri datas. Hum Brain Map 1998;6:339–47.

Streicher J, Weninger W, Müller G. External marker-based automatic congruencing: a new method of 3D reconstruction from serial sections. The Anatomical Record; 1997.

Thirion JP. Image matching as a diffusion process: an analogy with maxwell's demons. Med Image Anal 1998;2:243–60.

Thompson P, Toga A. A surface-based technique for warping three-dimensional images of the brain. IEEE Trans Med Imaging 1996;4:1–16.

Toga A, Ambach K, Schluender S. High-resolution anatomy from in situ human brain. Neuro Image 1994;1:334–44.

Toga A, Thompson P. Mapping brain asymmetry. Nat Rev Neurosci 2003;4:37–48.

Viola P, Wells WM. Alignment by maximization of mutual information. Int J Comp Vis 1997;24:137–54.

Zhao W, Young T, Ginsberg M. Registration and three-dimensional reconstruction of autoradiographic images by the disparity analysis method. IEEE Trans Med Imaging 1993;12:782–91.